

Modeling and Algorithms of Device Simulation for Ultra-High Speed Devices

Hideki Mutoh

Link Research Corporation
Odawara, Kanagawa, Japan
hideki.mutoh@nifty.com

Abstract— The physical models and algorithms of device simulation for ultra-high speed devices are proposed. The propagation of electromagnetic field induced by electrodes cannot be ignored for analyses of ultra-high speed devices. In order to obtain the consistent basic equations for the both of device and electromagnetic field propagation simulations, we newly introduce Nakanishi-Lautrup (NL) field of quantum electrodynamics (QED) to the electromagnetic field model. The models and algorithms are reported with some calculation results.

Keywords—ultra-high speed; field propagation; Nakanishi-Lautrup field; carrier generation; device simulation

I. INTRODUCTION

Operating speed of MOS transistors has been increased with reduction of their channel length. Some types of ultra high-speed semiconductor devices with more than 100 GHz operating frequency have been developed in the past several years [1]. The propagation of electromagnetic field induced by gate driving pulse cannot be ignored in such devices. In order to consider the propagation of electromagnetic field, device simulation for ultra-high speed devices should be based on Maxwell's equations instead of Poisson's equation. However, Maxwell's equations have the serious problems that carrier generation-recombination and charge injection from electrodes are prohibited by the equations.

Maxwell's equations are given by

$$\mathbf{J} = \nabla \times \mathbf{H} - \varepsilon \frac{\partial \mathbf{E}}{\partial t}, \quad (1)$$

$$\rho = \varepsilon \nabla \cdot \mathbf{E}, \quad (2)$$

$$\nabla \times \mathbf{E} + \mu \frac{\partial \mathbf{H}}{\partial t} = 0, \quad (3)$$

$$\nabla \cdot \mathbf{H} = 0, \quad (4)$$

where ρ is charge density, \mathbf{J} is current density, \mathbf{H} is magnetic field vector, \mathbf{E} is electric field vector. ε and μ are permittivity and permeability, which satisfy $\varepsilon \mu = 1/c^2$, where c denotes speed of light in the material. Equations (1) and (2) give the equation of charge conservation,

$$\nabla \cdot \mathbf{J} + \frac{\partial \rho}{\partial t} = 0. \quad (5)$$

Device simulations are ordinarily based on Poisson's and current continuity equations [2,3]

$$\varepsilon \nabla^2 \psi = -q(N_D - N_A + p - n), \quad (6)$$

$$\nabla \cdot \mathbf{J}_p + q \frac{\partial p}{\partial t} = GR, \quad (7)$$

$$\nabla \cdot \mathbf{J}_n - q \frac{\partial n}{\partial t} = -GR, \quad (8)$$

where ψ is potential, p and n are hole and electron concentration, N_D and N_A are donor and acceptor ion concentration, \mathbf{J}_p and \mathbf{J}_n are hole and electron current density, q is magnitude of electronic charge, and GR is the carrier generation-recombination rate. Equation (6) should be substituted by (1)-(4) to consider electromagnetic field propagation.

Since Maxwell's equations satisfy the principle of superposition [4], holes and electrons must individually satisfy (1) and (2). Then,

$$\mathbf{J}_p = \nabla \times \mathbf{H}_p - \varepsilon \frac{\partial \mathbf{E}_p}{\partial t}, \quad (9)$$

$$\rho_p \equiv qp = \varepsilon \nabla \cdot \mathbf{E}_p, \quad (10)$$

where \mathbf{H}_p and \mathbf{E}_p are magnetic and electric fields induced by holes, respectively. Therefore, (7) is not satisfied in the case of $GR \neq 0$, because (9) and (10) give

$$\nabla \cdot \mathbf{J}_p + \frac{\partial \rho_p}{\partial t} = 0. \quad (11)$$

Since the above situation is same for electrons, carrier generation and recombination are forbidden by Maxwell's equations. In addition to the above problem, electrode regions in device simulation do not satisfy the charge conservation. In silicon, current injection and absorption at electrode surfaces give $\nabla \cdot \mathbf{J} \neq 0$ even in the steady state of $\partial \rho / \partial t = 0$. Gate electrodes also do not satisfy (5) in transient analysis, because gate surfaces give $\nabla \cdot \mathbf{J} = 0$ and $\partial \rho / \partial t \neq 0$ when time dependent voltage is applied to the gate. Consequently, modification of Maxwell's equations is needed by the device simulation with considering electromagnetic field propagation to treat carrier generation-recombination and charge creation-annihilation at electrode surfaces.

II. MODIFICATION OF MAXWELL'S EQUATIONS

Using vector potential \mathbf{A} and scalar potential ψ , electric field vector \mathbf{E} and magnetic field vector \mathbf{H} are written as

$$\mathbf{E} = -\nabla\psi - \frac{\partial\mathbf{A}}{\partial t}, \quad (12)$$

$$\mathbf{H} = \frac{1}{\mu}\nabla\times\mathbf{A}. \quad (13)$$

In order to realize current injection and absorption at electrode surfaces and carrier generation-recombination in semiconductors, we introduce Nakanishi-Lautrup (NL) field B and a gauge parameter α , which was introduced for quantum electrodynamics (QED) [5-7]. The Lagrangian density of the electromagnetic field L is given by [6, 8]

$$L = -\frac{1}{4}F^{\nu\lambda}F_{\nu\lambda} + B\partial^\nu A_\nu + \frac{1}{2}\alpha B^2 - \mu J^\nu A_\nu, \quad (14)$$

where J^ν and A^ν denote 4-D current ($c\rho$, \mathbf{J}) and 4-D potential (ψ/c , \mathbf{A}), respectively, and $F^{\nu\lambda}$ is given by

$$F^{\nu\lambda} = \partial^\nu A^\lambda - \partial^\lambda A^\nu. \quad (15)$$

The Lagrangian density (14) gives the following equations.

$$\mu J_\nu = \square A_\nu - \partial_\nu \partial^\lambda A_\lambda - \partial_\nu B, \quad (16)$$

$$\alpha B + \partial^\nu A_\nu = 0, \quad (17)$$

where \square is d'Alembertian defined by

$$\square \equiv -\nabla^2 + \frac{1}{c^2} \frac{\partial^2}{\partial t^2}. \quad (18)$$

Equations (1) and (2) are rewritten by using (12), (13), and (16) as

$$\mathbf{J} = \nabla\times\mathbf{H} - \varepsilon \frac{\partial\mathbf{E}}{\partial t} + \frac{1}{\mu}\nabla B, \quad (19)$$

$$\rho = \varepsilon\nabla\mathbf{E} - \varepsilon \frac{\partial B}{\partial t}. \quad (20)$$

Therefore, the carrier generation-recombination rate is given by

$$GR = \nabla\mathbf{J} + \frac{\partial\rho}{\partial t} = -\frac{1}{\mu}\square B. \quad (21)$$

The above relation permits current injection and absorption at electrode surfaces and carrier generation-recombination in semiconductors. It should be noticed that $GR = 0$ needs not $B = 0$ but $\square B = 0$. Although $\square B = 0$ is always assumed in QED, we assume $\square B \neq 0$ in the region of $GR \neq 0$.

III. SIMULATION ALGORITHM FOR FIELD PROPAGATION

It is difficult to consider the propagation of magnetic field induced by gate electrodes, because of complexity of current calculation in gate electrodes. If we consider only electric and NL fields, the simulation of the field propagation is much simpler than the above case, by assuming

$$|\nabla\times\mathbf{H}| \ll \left| \varepsilon \frac{\partial\mathbf{E}}{\partial t} - \frac{1}{\mu}\nabla B \right|. \quad (22)$$

Then, electromagnetic field propagation can be calculated by considering only electric and NL fields [9]. When we introduce conductivity σ and use $\mathbf{J} = \sigma\mathbf{E}$, the discretization of the fields can be done by FDTD method [10] as

$$\begin{aligned} B^{n+1/2}(i, j, k) &= B^{n-1/2}(i, j, k) - \frac{\Delta t}{\varepsilon} \rho(i, j, k) \\ &+ \frac{\Delta t}{\Delta x} \{E_x^n(i+1/2, j, k) - E_x^n(i-1/2, j, k)\} \\ &+ \frac{\Delta t}{\Delta y} \{E_y^n(i, j+1/2, k) - E_y^n(i, j-1/2, k)\} \\ &+ \frac{\Delta t}{\Delta z} \{E_z^n(i, j, k+1/2) - E_z^n(i, j, k-1/2)\}, \quad (23) \end{aligned}$$

$$\begin{aligned} E_x^{n+1}(i+1/2, j, k) &= \frac{1 - \frac{\sigma}{2\varepsilon}\Delta t}{1 + \frac{\sigma}{2\varepsilon}\Delta t} E_x^n(i+1/2, j, k) \\ &+ \frac{c^2\Delta t}{\Delta x \left(1 + \frac{\sigma}{2\varepsilon}\Delta t\right)} \{B^{n+1/2}(i+1, j, k) - B^{n+1/2}(i, j, k)\}, \quad (24) \end{aligned}$$

$$\begin{aligned} E_y^{n+1}(i, j+1/2, k) &= \frac{1 - \frac{\sigma}{2\varepsilon}\Delta t}{1 + \frac{\sigma}{2\varepsilon}\Delta t} E_y^n(i, j+1/2, k) \\ &+ \frac{c^2\Delta t}{\Delta y \left(1 + \frac{\sigma}{2\varepsilon}\Delta t\right)} \{B^{n+1/2}(i, j+1, k) - B^{n+1/2}(i, j, k)\}, \quad (25) \end{aligned}$$

$$\begin{aligned} E_z^{n+1}(i, j, k+1/2) &= \frac{1 - \frac{\sigma}{2\varepsilon}\Delta t}{1 + \frac{\sigma}{2\varepsilon}\Delta t} E_z^n(i, j, k+1/2) \\ &+ \frac{c^2\Delta t}{\Delta z \left(1 + \frac{\sigma}{2\varepsilon}\Delta t\right)} \{B^{n+1/2}(i, j, k+1) - B^{n+1/2}(i, j, k)\}, \quad (26) \end{aligned}$$

where i, j, k , and n denote the grid node addresses along x, y, z , and time axes, respectively. $\Delta x, \Delta y, \Delta z$, and Δt are the grid spaces along x, y, z , and time axes, respectively. B is defined on the middle time point between the time grids on which ψ and \mathbf{E} are defined. When we assume $\alpha = 1$ and $\nabla\mathbf{A} = 0$, the boundary condition on the electrode surface is given by (17) as

$$B^{n+1/2}(i_e, j_e, k_e) = -\frac{\psi^{n+1}(i_e, j_e, k_e) - \psi^n(i_e, j_e, k_e)}{c^2\Delta t}, \quad (27)$$

where i_e, j_e , and k_e denote the grid node addresses of electrode surface, and $\psi^n(i_e, j_e, k_e)$ and $\psi^{n+1}(i_e, j_e, k_e)$ are given by the electrode voltage condition. We can obtain B and \mathbf{E} by alternately substituting them to (23)-(26), after calculating $B^{n+1/2}(i_e, j_e, k_e)$ by (27) in every time step. The transient analysis of device simulation including electromagnetic field propagation can be achieved by solving current continuity equations (7) and (8) at the appropriate time grids with obtaining the potential distribution by the above method. The above models and algorithms were implanted into 3-D device simulator SPECTRA [11-13], which performed the following analyses.

IV. DEVICE SIMULATIONS CONSIDERING ELECTROMAGNETIC FIELD PROPAGATION

A. 1-D field propagation analysis

The analyzed structure and the gate pulse shape are shown in Fig. 1 (a) and (b), where τ_f denotes the fall time of driving pulse. Fig 1 (c)-(h) show the electric (blue solid) and NL (red broken) field distribution along depth direction at t of 0.04, 0.12, 0.24, 0.36, 0.48, and 0.6 ps in the case of $\tau_f = 0.1$ ps.

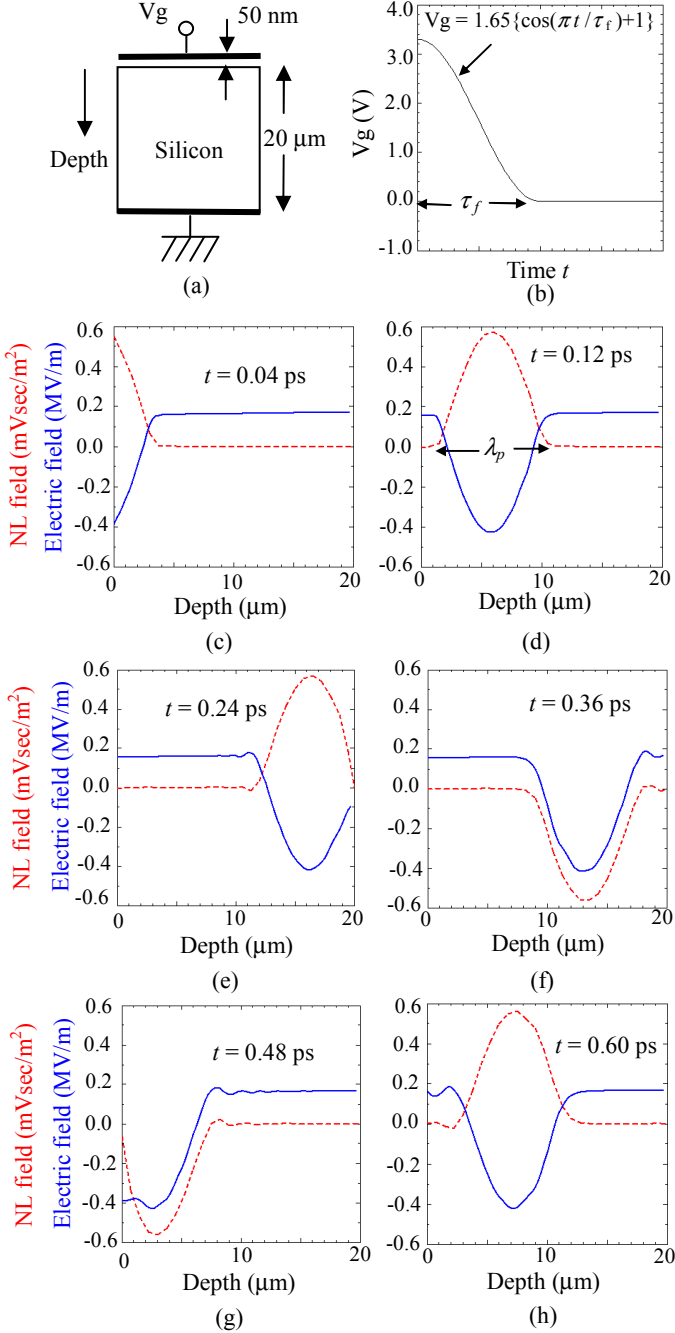


Fig. 1. 1D simulation result of electric field and NL field distribution dependence on time, where λ_p denotes the wave packet length (Blue solid line: electric field, Red broken line: NL field). (a) Analyzed structure. (b) V_g dependence on time. (c) $t = 0.04$ ps. (d) $t = 0.12$ ps. (e) $t = 0.24$ ps. (f) $t = 0.36$ ps. (g) $t = 0.48$ ps. (h) $t = 0.60$ ps.

The sign of the NL field is changed by every reflection at the gate and substrate electrodes. Since the absorption coefficient is very small for the wavelength more than $1 \mu\text{m}$, the NL field wave packet induced by gate electrode driving pulse exists in the silicon substrate for long time, by multi-reflection of the gate and substrate electrodes. Since the wave packet length λ_p is given by $c\tau_f$, $\tau_f = 0.1$ ps gives $\lambda_p = 9 \mu\text{m}$ in silicon and $\lambda_p = 30 \mu\text{m}$ in vacuum.

B. Readout potential analysis for CMOS image sensor

Fig. 2 (a) shows the 2D analyzed structure of CMOS image sensor including a photodiode (PD), a transfer gate (TG), and a floating diffusion (FD). The transfer gate voltage (V_{TG}) is changed from 0 to 3.3 V with rise time τ_r as shown in Fig. 2 (b). The potential distribution with $\tau_r = 0.1$ ps at $t = 0.14$, 0.24, and 0.34 ps are shown in Fig. 2 (c), (d), and (e), respectively.

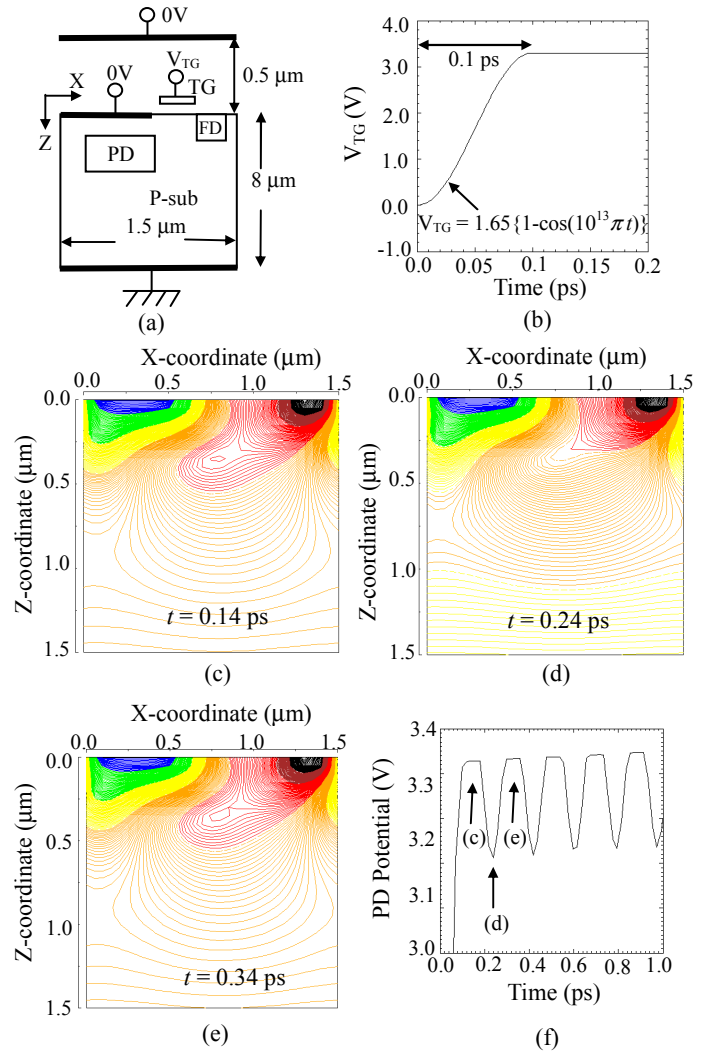


Fig. 2. CMOS image sensor potential distribution dependence on time, drawn by 25 mV step contour lines. (a) Analyzed structure. (b) V_{TG} dependence on time. (c) $t = 0.14$ ps. (d) $t = 0.24$ ps. (e) $t = 0.34$ ps. (f) PD maximum potential dependence on time in the region of $0.5 \leq x \leq 0.75$ and $0.25 \leq z \leq 0.5$.

Although the potential well of photodiode region is collapsed at $t = 0.24$ ps, it is recovered at $t = 0.34$ ps. Fig. 2 (f) shows the maximum potential dependence on time in the region of $0.5 \leq x \leq 0.75$ and $0.25 \leq z \leq 0.5$. The potential vibration is caused by the electromagnetic wave packet induced by the transfer gate driving pulse, which is reflected by the top and backside electrodes.

C. Floating diffusion amp (FDA) noise analysis

Fig. 3 (a) shows the 2D structure including a floating diffusion (FD) and a gate electrode. The potential vibration amplitude dependence on the fall time τ_f of the gate driving pulse and the substrate thickness d_{sub} is calculated. The driving pulse shape is same as Fig. 1 (b). Fig. 3 (b) shows the FD potential dependence on time at $x = z = 0$ for $\tau_f = 0.2$ ps and $d_{sub} = 10 \mu\text{m}$. Fig. 3 (c) shows the potential vibration amplitude dependence on the fall time and the substrate thickness. The vibration amplitude steeply decreases with reduction of the substrate thickness in the case of $d_{sub} < \lambda_p/2$, although it is nearly constant in the case of $d_{sub} \geq \lambda_p/2$, where λ_p denotes the wave packet length as shown in Fig. 1 (d). This is explained by the interference of the wave packet.

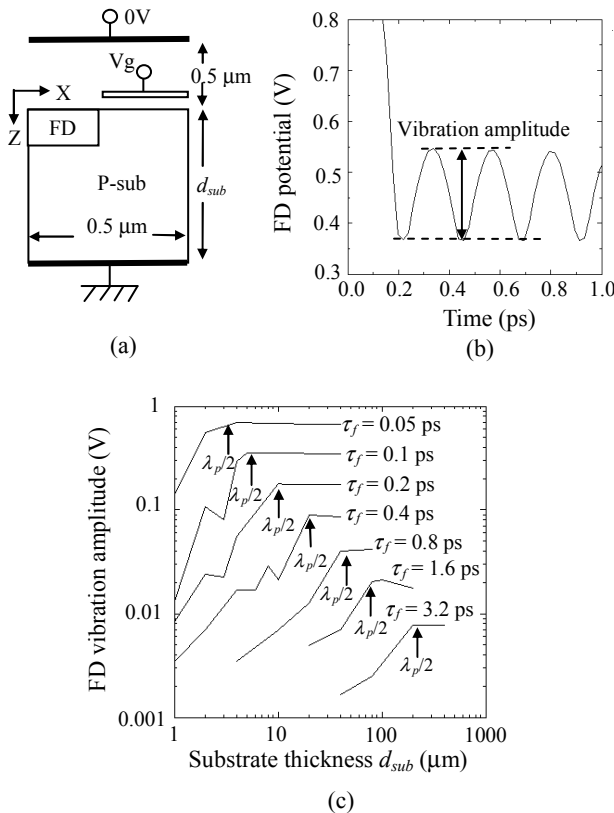


Fig. 3. Floating diffusion (FD) potential vibration dependence on time, where V_g is same as Fig. 1 (a). (a) Analyzed structure. (b) FD potential dependence on time at $x = z = 0$ for $\tau_f = 0.2$ ps and $d_{sub} = 10 \mu\text{m}$. (c) FD potential vibration amplitude dependence on the fall time τ_f and substrate thickness d_{sub} at $x = z = 0$. The arrows show half of λ_p , which is the wave packet length as shown in Fig. 1 (d).

It is shown that the vibration amplitude in the region of $d_{sub} \geq \lambda_p/2$ is almost proportional to $1/\tau_f$, because the maximum power of wave packet is proportional to $1/\tau_f$ if its energy is constant. It seems that the FDA noise caused by the driving pulses can be reduced by decreasing the substrate thickness. This result suggests that substrate thickness is an important factor for the noise characteristics of ultra-high speed devices.

V. CONCLUSION

The device simulation method with electromagnetic field propagation models including NL field is proposed for ultra-high speed device analysis. The readout characteristics of an ultra-high speed image sensor and noise characteristics of FDA were simulated by this method. It was found that the potential in the ultra-high speed device is vibrated by the electromagnetic field wave packet reflected by the front and backside of the substrate and the FDA noise induced by the gate driving pulse strongly depends on the pulse speed and the substrate thickness. The substrate thickness is an important factor for the noise characteristics of ultra-high speed devices.

REFERENCES

- [1] S. Gharavi and B. Heydari, *Ultra High-Speed CMOS Circuits*, Springer, 2011.
- [2] S. M. Sze, *Physics of Semiconductor Devices*, Wiley, New York, 1981.
- [3] S. Selberherr, *Analysis and simulation of semiconductor devices*, Springer, Wien, 1984.
- [4] R. P. Feynman, R. B. Leighton, and M. L. Sands, *Feynman Lectures on Physics 2*, Addison-Wesley, 1965.
- [5] N. Nakanishi, *Progr. Theor. Phys.*, vol. 35, 1111, 1966.
- [6] N. Nakanishi, *Ba-No-Ryoshiron (Quantum field theory)*, Baifukan, in Japanese, 1975.
- [7] I. J. R. Aitchison, *An informal introduction to gauge field theories*, Cambridge University Press, 1982.
- [8] H. Mutoh: "Confinement of charge creation and annihilation centers by Nakanishi-Lautrup field," viXra, (hep) 1403_0118, March 2014. <http://vixra.org/pdf/1403.0118v1.pdf>
- [9] H. Mutoh: "Physical Models and Algorithms for Device Simulation for High-Speed Image Sensors," *J. Institute of Image Information and Television Engineers*, vol. 67, no. 3, pp. J89-J94, 2013. https://www.jstage.jst.go.jp/article/itej/67/3/67_J89/_pdf
- [10] A. Taflov, *Computational Electrodynamics: The Finite-Difference Time-Domain Method*, Artech House, Norwood, MA, 1995.
- [11] H. Mutoh: "Simulation for 3-dimensional optical and electrical analysis of CCD," *IEEE Trans. Electron Devices*, vol. 44, pp. 1604-1610, 1997.
- [12] H. Mutoh: "3-D Optical and Electrical Simulation for CMOS Image Sensors," *IEEE Trans. Electron Devices*, vol. 50, pp. 19-25, 2003.
- [13] H. Mutoh, "Device simulation with electromagnetic field propagation models for high-speed image sensors and FDA noise analysis," *Proceedings of the 2013 international image sensor workshop*, 2013, https://www.imagesensors.org/Past%20Workshops/2013%20Workshop/2013%20Papers/07-01_052-Mutoh_paper.pdf